

Study on crystallization phenomenon and thermal stability of binary Ni–Nb amorphous alloy

S. Lesz¹ · G. Dercz²

Received: 17 January 2016 / Accepted: 17 August 2016 / Published online: 31 August 2016
© The Author(s) 2016. This article is published with open access at Springerlink.com

Abstract In this paper, a ribbon of binary Ni–Nb amorphous alloy was prepared by the melt spinning technique. Glass transition and crystallization phenomenon of the alloy were investigated by differential scanning calorimetry. Thermal properties of the ribbon of binary Ni–Nb upon heating and cooling were analysed by DTA at a heating/cooling rate of 0.5 K s^{-1} under the purified argon atmosphere. The thermal stability of Ni–Nb amorphous alloy was studied by using an X-ray diffractometer equipped with an in situ heating system. The structure and fracture morphology of the ribbons were examined by X-ray diffraction and scanning electron microscopy methods.

Keywords Amorphous alloy · Crystallization behaviours · Thermal properties

Introduction

Manufacturing is the process of transforming raw materials into products. The selection of a material decides often selection of manufacturing processes that may be used for producing elements from the selected material. Variety of materials available nowadays makes it necessary to select them properly for the constructional or functional elements,

tools and other products. Determining the relationships among structure, technological process, and functional properties, and also the selection of materials and technological processes forming their structure and properties for a use in manufacturing systems, feature the main focus of materials engineering. Materials and manufacturing engineering is interdisciplinary and focuses on the application of materials as well as process and production technologies in high-tech products within various fields, including energy production, the automotive and aeronautical industries, medicine and electronics, etc. [1–3].

In the case of applying adequate rates of cooling pass over from the liquid to the solid state with an amorphous structure, metals and alloys can be found in metallic glass. The amorphous structure can be obtained in pure metals and in binary, ternary and multicomponent alloys. These alloys are diversified in respect of chemical composition. The base of these alloys can be a combination of metal elements—non-metal and metal–metal. The chemical composition determines the glass-forming ability (GFA) of alloys. Depending on GFA, different geometric forms of these materials exist.

Due to the attained geometrical shape, metallic glass is divided into conventional and bulk metallic glass. In the process of casting conventional metallic glass, the cooling rate is 10^4 – 10^6 K s^{-1} [4].

The production of metallic glass is a complicated process, requiring the determination of the technological parameters. The results of investigations indicate that from the technological parameters, the linear velocity of the copper wheel and the temperature of casting affect the thickness of the amorphous ribbons most crucially [5, 6]. The technological parameters of manufacturing glass alloy affect the structure and adequate properties of the final products. Various methods of getting metallic glass are

✉ S. Lesz
Sabina.lesz@polsl.pl

¹ Institute of Engineering Materials and Biomaterials, Silesian University of Technology, 18a Konarskiego Street, 44-100 Gliwice, Poland

² Institute of Materials Science, University of Silesia, 1A, 75 Pułku Piechoty Street, 41-500 Chorzów, Poland

practically applied, the common feature of which is the necessity of warranting such a cooling rate that permits the liquid alloy to consolidate to a glassy state. The most commonly applied method of producing metallic glass is the method of continuous casting of the liquid alloy on the surface of a rotating cooper wheel. Methods of fabrication of metallic glass depend on the size and shape of the nozzle of the crucible. When the shape is circular—the method is called melt spinning, and if square—planar flow casting method. These methods are limited to the fabrication of conventional metallic glass in the shape of ribbons. The thickness of the obtained ribbons is in the range from 0.02 to 0.06 mm. Thus, the range of application of metallic glass in the form of ribbons is limited because of their dimensions [5–7].

The adequate chemical composition of the rapidly quenched alloy permits to control properties, e.g. magnetic and mechanical. The alloys consisting of Fe, Co, Ni and their combination in the chemical composition belong to ferromagnetic metallic glass having a specific application. Doping alloy with elements, like Cr, Nb, Ti, Hf, Mo, Mn, Al, Ta and others has a significant influence on the magnetic and electrical properties, and application is obtained [5].

Investigations concerning the technique of producing metallic glass and its properties, which have been carried out for many years, resulted in the production of the so-called bulk metallic glass (BMG) with different geometrical form (ribbons/plates, rods, tubes) and various dimensions (thickness, diameter, full and inside diameter). When lower cooling rates are applied, from 10^6 to 1 K s^{-1} , the thickness of the ribbons is in the range 0.1–100 mm [5]. BMG is obtained by means of casting methods applied in the production of crystalline materials. The following methods are to be distinguished: continuous and discontinuous, vacuum and pressure casting, gravitational and centrifugal casting. Depending on the applied method of fabricating (the parameters of the apparatus) alloy different structures (amorphous, crystalline) can be obtained. The empirical rules of the production of bulk metallic glass indicate that the more component elements are applied, the more difficult it becomes to diffuse the atoms in the course of cooling [8–11]. It becomes difficult to diffuse atoms in the course of cooling, and thus the nucleation and crystallization can be depressed, resulting in the increase in the undercooling of alloy melt. The mentioned process improves GFA.

A large amount of components in the alloys hampers investigations as well as the simulation of the glass-forming ability and also investigations concerning structural correlations. Therefore, investigations have been started on binary bulk metallic glasses produced by different method (ribbons, rods). In 2004, bulk Cu–Zr alloys with a thickness of up to a critical 2 mm were developed [12].

Subsequently, Pd–Si binary bulk metallic glasses with a diameter of 6 mm were reported to be prepared [13]. At the same time, glassy alloys Ni–Nb alloy were prepared [14]. The Ni–Nb type alloy has thanks to its easy and relatively inexpensive production proved to be an interesting and promising example of binary metallic glass. From the thermodynamic point of view, Ni–Nb binary alloys provide an ideal model system for the study of the GFA [4, 15].

Ni-based metallic glasses display a high thermal stability, high compressive strength, a good plasticity and also high corrosion resistance [4, 9, 10, 16, 17]. Casting (using the pressure die casting method) Ni–Nb alloys in rod form with diameters 2 and 3 mm according to thermodynamic principles has high GFA. The results of differential scanning calorimetry obtained from amorphous $\text{Ni}_{62}\text{Nb}_{38}$ rods with a diameter 2 mm, at a heating rate 0.33 K s^{-1} indicate that the temperature of glass transition— T_g is equal to 892 K and the temperatures of the first and second stage of crystallization— T_{x1} and T_{x2} are, respectively, 932 K and 981 K. The liquidus temperature— T_l for the amorphous rod is about 1483 K. Therefore, the reduced glass transition temperature— T_{rg} ($T_{rg} = (T_g/T_l)$) and parameter γ ($\gamma = T_{x1}/(T_g + T_l)$), which is employed to reflect the GFA of the alloys, is about 0.60 and 0.392 [4, 5, 18].

GFA of $\text{Ni}_{62}\text{Nb}_{38}$ alloy can be described by the calculated fragility parameter— m , determined by Angell's conception is about 28 [4]. Novikov and Sokolov have revealed that the fragility of a glass-forming liquid— m , is strictly linked to a very basic property such as Young's elastic modulus— E . The elastic modulus E can be evaluated from [19]: $T_g/E \propto m$. The $\text{Ni}_{62}\text{Nb}_{38}$ BMG alloy may have a higher elastic modulus because it has a much higher value T_g and a slightly lower value of m than most of other BMG [4, 19]. Furthermore, according to conceptual approach to evaluate the strength of metallic glasses proposed by Yang, the fracture strength of $\text{Ni}_{62}\text{Nb}_{38}$ alloy could reach about 4 GPa [20]. The nano-indentation and compression testing results have proved that the $\text{Ni}_{62}\text{Nb}_{38}$ BMG alloys have high hardness—15 GPa, and highest Young's modulus—231 GPa and fracture strength 3.1 GPa among binary BMGs [4, 14, 16, 21, 22]. The better GFA among $\text{Ni}_{61.5}\text{Nb}_{38.5}$, $\text{Ni}_{62}\text{Nb}_{38}$, $\text{Ni}_{62.5}\text{Nb}_{37.5}$ alloys with chemical composition near to the eutectic composition is observed for $\text{Ni}_{62}\text{Nb}_{38}$ [16]. Among these alloys, only $\text{Ni}_{62}\text{Nb}_{38}$ rod with diameter 2 mm has amorphous structure. In the structure of the $\text{Ni}_{62}\text{Nb}_{38}$ rod with a diameter above 2 mm crystalline phases are formed [16]. Therefore, the critical diameter for $\text{Ni}_{62}\text{Nb}_{38}$ BMG should be less than 3 mm [4, 16].

Binary Ni–Nb alloys are characterized by good castability and solidification shrinkage. Metallic glasses obtained from these alloys are characterized by low porosity, a high thermal stability, high compressive strength, a good plasticity and also high corrosion

resistance. The superior surface imprintability, net-shape forming capability and high repeatability have been found to be very functional in the field of micro-machines, for example advanced medical equipment, i.e. endoscopes, micro-pump, catheter for thrombus removal [5]. Since functional properties are highly dependent on structure, detailed understanding of crystallization phenomenon and thermal stability is very important to continue developing new materials with controlled properties. The aim of this work is to determine the boundary parameters of the materials permitting the attainment of an amorphous structure of products with a given geometrical shape (ribbons) and dimensions made of binary Ni–Nb alloys. The boundary parameters of the material comprise, among others, the glass-forming ability (GFA), connected with the glass transition temperature— T_g , critical cooling rate (R_c) and critical section thickness (Z_c) of the $Ni_{62}Nb_{38}$ ribbon. Time–temperature stability is especially important in terms of the utilization of this group of amorphous alloys.

Experimental

Investigations were carried out on an amorphous alloy with compositions of $Ni_{62}Nb_{38}$. The ingot of Ni–Nb binary mother alloy (alloy composition is given in nominal at.%) was prepared by induction melting using the TECHMA-ELCAL Typ-Rel 15 furnace of which the mixtures of pure Ni (99.98 mass%) and Nb (99.95 mass%) were used in a high purity argon atmosphere. The composition was confirmed by energy-dispersive X-ray spectroscopy (EDX) quantification in scanning electron microscopy (SEM).

The investigated material was cast in form of the ribbons. The investigated materials were cast as ribbon-shaped metallic glasses with a thickness (g) 0.05 mm and width (d) 4 mm. The ribbons were manufactured by the melt spinning technique using the UFA-2 ZDEMP-IM5 system, which is a method of continuous casting of the liquid alloy on the surface of a turning copper based wheel [23, 24]. The master alloy was melted in a quartz crucible using an induction coil and pushed thereafter on a copper wheel. The casting conditions include linear speed of copper wheel of 20 m s^{-1} and an ejection over-pressure of molten alloy under an argon atmosphere of 0.02 MPa.

The thermal stability associated with the glass transition temperature (T_g), crystallization (T_x), liquidus melting temperature (T_l) and peak (T_x) crystallization temperature was examined with a differential scanning calorimeter (DSC, Perkin-Elmer DSC7) at heating rate of 0.33 K s^{-1} and differential thermal analyser (DTA, Perkin-Elmer DTA7) at heating/cooling rate of 0.5 K s^{-1} , under the purified argon atmosphere. The T_g is defined as the mid-height point of the endothermic event for glass

transition. The DTA and DSC measurements were carried out with a NETZSCH model DSC 404 C Pegasus. The thermal stability of Ni–Nb amorphous alloy was studied by using an X-ray diffractometer (X'pert Pro diffractometer with Philips X'celerator detector) equipped with an in situ heating system (Anton Paar HTK—2000 in situ high temperature camera). The measurements were performed under high vacuum at temperatures ranging from 373 to 1273 K.

Several parameters have been used to determine the glass-forming ability of $Ni_{62}Nb_{38}$ alloy. The first one is a parameter defined as the reduced glass transition temperature (T_{rg}). The reduced glass temperature $T_{rg} (= T_g/T_l)$ is [25]:

$$T_{rg} = T_g/T_l \quad (1)$$

where T_g is the temperature of glass transition, and T_l is the liquidus temperature.

The temperature interval ΔT_x between the glass transition temperature (T_g) and the onset crystallization temperature (T_x) is another glass-forming ability indicator [26]:

$$\Delta T_x = T_x - T_g \quad (2)$$

This parameter is also called as the super-cooled liquid region. It is obviously known that the larger the temperature interval, the higher the glass-forming ability [26]. Last parameter (γ) defined as [27]:

$$\gamma = T_{x1}/T_g + T_l \quad (3)$$

for judging, GFA among metallic glasses has been proposed from the perspectives of both amorphization and devitrification processes [27]. Regardless of alloy system, the relationship between (γ) and the critical cooling rate (R_c) as well as critical section thickness (Z_c) has been formulated as follows [18]:

$$R_c = 5.1 \times 10^{21} \exp(-117.19\gamma) \quad (4)$$

and

$$Z_c = 2.80 \times 10^{-7} \exp(41.70\gamma) \quad (5)$$

Note that these two equations can be utilized to estimate R_c and Z_c when γ is measured readily from DSC/DTA measurements [18]. R_c is in K s^{-1} , γ is dimensionless, and Z_c is in millimetres. Structure and fracture morphology of the ribbons were examined by X-ray diffraction (XRD) and scanning electron microscopy (SEM) methods. Structure analysis of studied materials in as-cast state was carried out using X-ray diffractometer (XRD) method on a X-Pert PRO MP diffractometer using filtered $\text{CoK}\alpha$ radiation ($\lambda = 0.17888 \text{ nm}$). The data of diffraction lines were recorded by “step-scanning” method in 2θ range from 35° to 90° from the area A—the air-side surface (top row), and from the area C—the wheel-side surface (bottom row) of ribbons. Phase qualitative analysis was performed using of

classical X-ray diffraction. X-Ray Diffraction (XRD) can be used to determine phase composition (commonly called phase ID) for mixtures of crystalline and nanocrystalline metals, foils, coatings and films, etc. [28]. The result of analysis consists of identified phase list with experimentally observed X-ray patterns and known diffraction patterns from various sources. The sources and the notation describing the quality of data are maintained by the ICDD (International Centre for Diffraction Data) [29]. The peaks were compared to probable crystalline species using software X'Pert Highscore Plus correlated with the ICDD PDF 4+ database.

The chemical composition of ribbons was fixed by means of the point-by-point method, using energy-dispersive X-ray spectroscopy (EDX) produced by EDAX (TRIDENT XM4), which is a part of scanning electron microscope (SEM) equipment.

The morphology of fracture surfaces of the ribbons after decohesion was examined by means of the scanning electron microscope (SEM) SUPRA 25, ZEISS firm, with voltage of 20 kV. The studies were carried out on cross section of the ribbons in the areas: A—the air-side surface (top row), the upper (free) surface B—intermediate area, C—the wheel-side surface (bottom row), the lower surface.

Results and discussion

The thermal properties of the as-spun $\text{Ni}_{62}\text{Nb}_{38}$ ribbon samples upon heating and cooling measured by DSC and DTA are presented on Figs. 1 and 2a, b, respectively.

The DSC curves of the as-spun $\text{Ni}_{62}\text{Nb}_{38}$ ribbon samples at a heating rate of 0.33 K s^{-1} are shown in Fig. 1. The trace exhibits an endothermic event characteristic of the glass transition and a super-cooled liquid region, followed

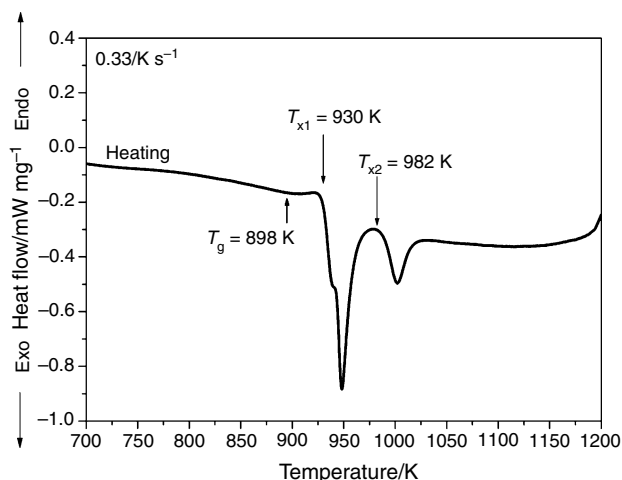


Fig. 1 Differential scanning calorimetry (DSC) curves of the $\text{Ni}_{62}\text{Nb}_{38}$ ribbon under the heating rate of 0.33 K s^{-1}

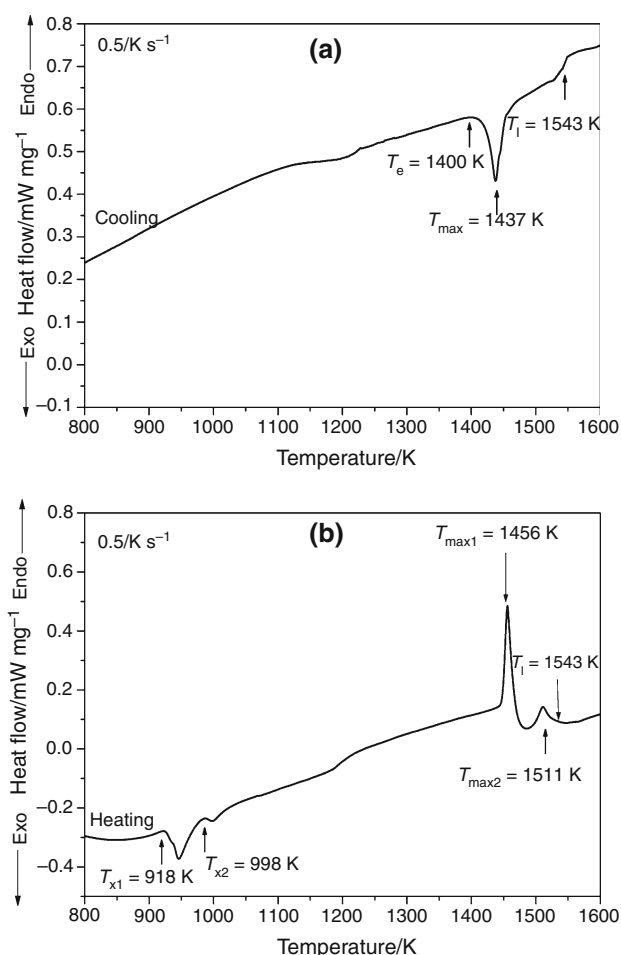


Fig. 2 Differential thermal analysis (DTA) curves of the $\text{Ni}_{62}\text{Nb}_{38}$ ribbon under the cooling (a) and heating (b) rate of 0.5 K s^{-1}

by two exothermic events characteristic of crystallization processes. A marked endothermic behaviour before crystallization demonstrates a distinct glass transition with the onset temperature T_g at about 898 K. Two sharp exothermic reactions occur after the glass transition associated with the transformations from super-cooled liquid state to the equilibrium crystalline intermetallic phases. The onset and peak temperatures for crystallizations T_{x1} and T_{x2} are about 930 and 948 K and 982 and 1002 K, respectively.

Figure 2a, b shows DTA curves of the $\text{Ni}_{62}\text{Nb}_{38}$ ribbon under the cooling (a) and heating (b) rate of 0.5 K s^{-1} . During heating, the sample exhibits a distinct endothermic peak due to glass transition, followed by a super-cooled liquid region, and then a sharp exothermic peak due to crystallization. With further increasing temperature, the alloys finally melt after several steps of endothermic events. The liquid temperature T_l for the alloy is about 1543 K (Fig. 2a, b). The curve of the $\text{Ni}_{62}\text{Nb}_{38}$ ribbon presents two-stage crystallization behaviour (two exothermic peaks: $T_{x1} = 918 \text{ K}$ and $T_{x2} = 998 \text{ K}$) (Fig. 2b).

Two endothermic melting peaks were observed for the $\text{Ni}_{62}\text{Nb}_{38}$ ribbon, indicating the composition is not pseudo-eutectic. The slight difference between the DSC and DTA calculated results ($T_{x1} = 930, 918 \text{ K}$ and $T_{x2} = 982, 998 \text{ K}$) could be due to different heating rate usage.

As presented in [30], the melt-spun amorphous $\text{Ni}_{60}\text{Nb}_{40}$ alloy showed a weak exothermic peak with onset and peak temperatures of 933 and 946 K, respectively, and strong exothermic peak with onset and peak temperatures of 987 and 1001 K, respectively.

Table 1 lists the results of thermal analysis: the glass transition temperature (T_g), crystallization temperature (T_{x1}), the liquidus temperature (T_l) and parameters for GFA—glass-forming ability: super-cooled liquid region (ΔT_x), the reduced glass transition temperature (T_{rg}), parameter (γ), the critical cooling rate (R_c) and critical section thickness (Z_c) of the $\text{Ni}_{62}\text{Nb}_{38}$ ribbon.

Therefore, the super-cooled liquid region ΔT_x , the reduced glass transition temperature T_{rg} and parameter γ , which are usually employed to reflect the GFA of the alloys, are about 32 K, 0.582, and 0.381. The critical cooling rate R_c and critical section thickness Z_c were predicted to be 207.29 K s^{-1} and 2.22 mm, respectively, which indicate the higher GFA of $\text{Ni}_{62}\text{Nb}_{38}$. According to [16], for the $\text{Ni}_{62}\text{Nb}_{38}$ alloy, the value of R_c and Z_c could be estimated to be 57 K s^{-1} and 3.5 mm, respectively.

Comparison of the obtained $T_g = 898 \text{ K}$ value of the investigated alloy shows that the value is higher than in alloy with the similar chemical composition investigated by Cheng whose results for $\text{Ni}_{60}\text{Nb}_{40}$ alloy was equal to $T_g = 891 \text{ K}$ [31]. This temperature is dependent on the heating rate, and it is important to utilize the same heating rate for the measurements. The slight differences could be due to the purity and natural elements. The shortage is that the glass-forming ability (GFA) of most developed binary Ni-based MGs is relatively low. With the addition of elements, like Zr [31] and Al [30, 32], the GFA can be obviously improved.

It was found that ΔT_x , alone cannot effectively reflect the relative GFA for metallic glasses [27]. Although the

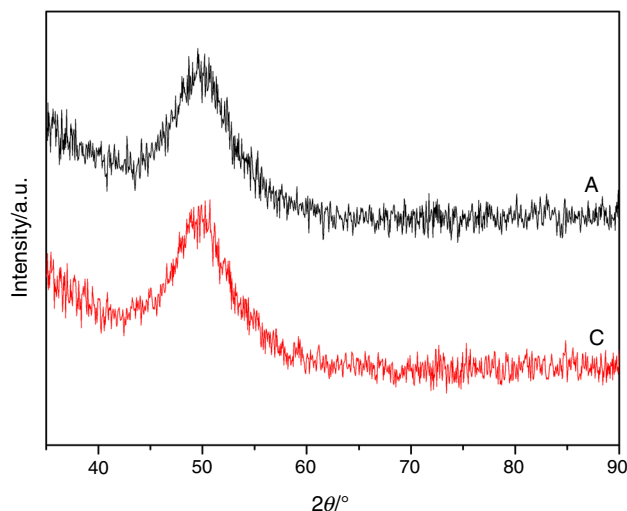


Fig. 3 X-ray diffraction pattern of the melt-spun $\text{Ni}_{62}\text{Nb}_{38}$ ribbons, area A—the air-side surface (top row) known as the upper (free) surface, area C—the wheel-side surface (bottom row), known as the lower surface

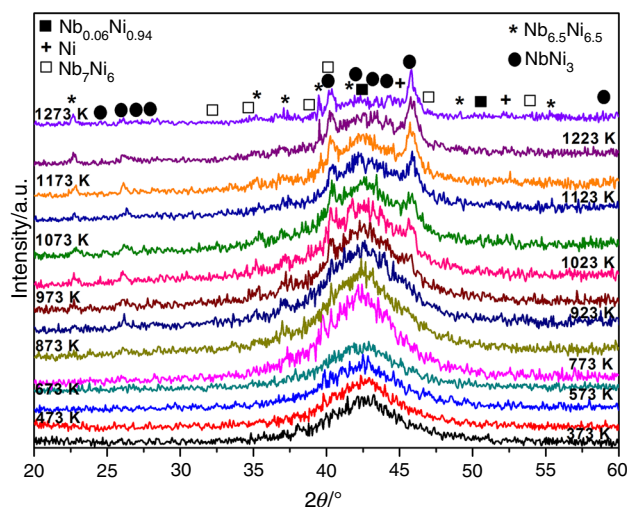


Fig. 4 X-ray diffraction pattern of $\text{Ni}_{62}\text{Nb}_{38}$ ribbon specimens annealed at different temperatures

Table 1 Thermal stability: the glass transition temperature (T_g), crystallization temperature (T_x), the liquidus temperature (T_l) and GFA: super-cooled liquid region ($\Delta T_x = T_{x1} - T_g$), the reduced glass transition temperature ($T_{rg} = T_g/T_l$), parameter ($\gamma = T_{x1}/T_g + T_l$), critical cooling rate ($R_c = 5.1 \times 10^{21} \exp(-117.19\gamma)$), critical section thickness ($Z_c = 2.80 \times 10^{-7} \exp(41.70\gamma)$) of the $\text{Ni}_{62}\text{Nb}_{38}$ ribbon

Samples	T_g/K	T_{x1}/K	T_{x2}/K	T_l/K	$\Delta T_x/\text{K}$	T_{rg}	γ	$R_c/\text{K s}^{-1}$	Z_c/mm
$\text{Ni}_{62}\text{Nb}_{38}$ ribbon	898	930	982	1543	32	0.582	0.381	207.29	2.22
$\text{Ni}_{60}\text{Nb}_{40}$ rod ($\phi = 1 \text{ mm}$)	891	924	981	1478	33	0.603	0.390	72.19	3.23

Also data of $\text{Ni}_{60}\text{Nb}_{40}$ bulk specimen with diameter of 1 mm are included for comparison. Thermal behaviour associated with glass transition (T_g), crystallization (T_x) and liquidus melting temperature (T_l) was examined with a DSC, at heating rate of 0.67 K s^{-1} and DTA, at heating rate of 0.33 K s^{-1} [30]

GFA of metallic glasses is somehow dependent on T_{rg} , parameter γ showed a stronger correlation with GFA than T_{rg} . This was confirmed by a higher R^2 value and a narrower prediction band for the γ —(R_c , Z_c) relation than those of T_{rg} —(R_c , Z_c). The newly defined gauge γ has been successfully applied to glass formation in the bulk Ni–Nb alloy system.

Thermodynamic analysis could be useful in evaluating the composition of a good glass former in more detail. Inoue and co-workers proposed a thermodynamic model to determine glass-forming compositions from empirical rules. However, because glass formation is always a competing process between super-cooled liquid and the resulting crystalline phase, the influence of the formation enthalpy of crystalline phases on the synthesis of metallic glasses should not be neglected. Lu and Liu have demonstrated that the GFA of the alloys depends not only on the liquidus and glass transition temperature but also on the stability of the competing crystalline phases [27].

Therefore, consideration of the thermal stability of Ni–Nb amorphous alloy could be very important for evaluating the glass formation and the crystallization process of metallic glasses. DTA/DSC testing methods were applied particularly to study the effects of nucleating agents in crystallizing systems [33]. Peaks in the DTA/DSC curve show the exothermic reactions taking place as species attain the activation energy necessary to incite crystallization, while endothermic minima have been attributed to glass transition and melting onset temperature. The DTA/DSC method does not identify which species are being grown without a supporting characterization method, such as X-ray diffraction. In order to identify the crystallization products of each exothermic reaction, heat treatments were performed under the following two conditions: (1) to complete the first exothermic reaction; and (2) to complete the second exothermic reaction by heating the as-quenched ribbon specimen to a predetermined temperature. The thermal stability of Ni–Nb amorphous alloy was studied by

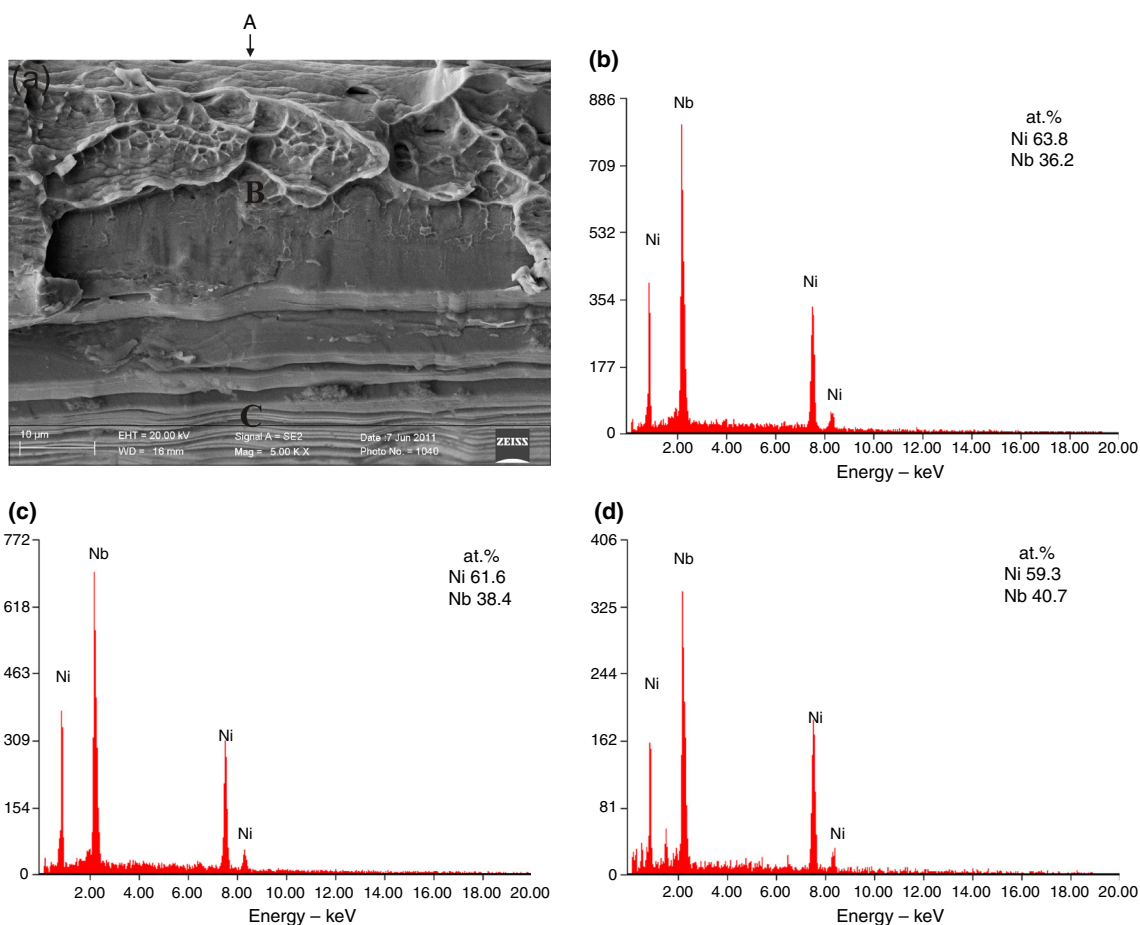


Fig. 5 SEM image of fracture morphology on the ribbon's cross section (a); area A—typical ductile fracture with vein pattern morphology of amorphous $Ni_{62}Nb_{38}$ ribbon in as-quenched state,

area B—smooth area with slight faults, area C—the narrow parallel faults as a result of the occurrence of shear bands; (b), (c), (d)—the places (A, B, C) of EDX analysis with results

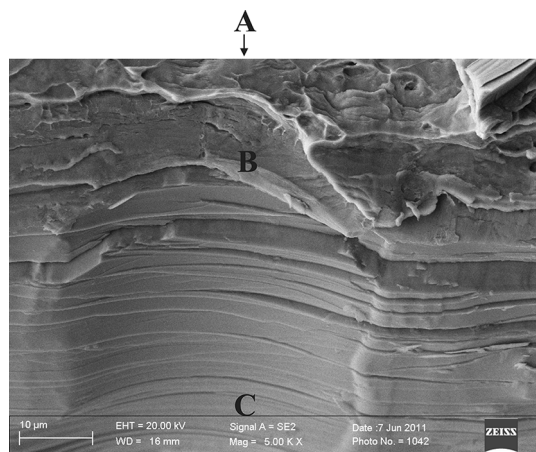


Fig. 6 SEM image of fracture morphology on the ribbon's cross section; area A—typical ductile fracture with vein pattern morphology of amorphous $\text{Ni}_{62}\text{Nb}_{38}$ ribbon in as-quenched, intermediate area B—smooth fracture with areas of shear bands, C—areas of shear bands

using an X-ray diffractometer equipped with an in situ heating system.

Figure 3 shows typical XRD-patterns obtained from the area A—the air-side surface (top row), and from the area C—the wheel-side surface (bottom row) of ribbons cast on a smooth wheel surface show a broad-angle peak, characteristic of amorphous structure, with no evidence of crystalline Bragg peaks (Fig. 3). The upper (free) surface was quite smooth and had shiny surface; the lower surface contained a large number of very small, irregular indentations that appear to have been caused by trapped gas bubbles, giving this surface a slightly matte appearance. But these visual differences are not observable in the obtained results of structural studies performed by X-ray diffraction.

Figure 4 shows X-ray diffraction patterns of $\text{Ni}_{62}\text{Nb}_{38}$ ribbons specimens annealed at different temperatures. The specimen heated to 673 K, above the first exothermic reaction, shows a broad diffraction pattern with a few unidentified weak peaks. Comparing with the as-quenched ribbon specimen, the width of the broad peak decreased. The specimen heated to 1023 K, above the second exothermic peak (982 K), showed several diffraction peaks, which can be analysed as a mixture of rhombohedral Nb_7Ni_6 and $\text{Nb}_{6.5}\text{Ni}_{6.5}$ phases with lattice constants of $a = 5.086 \text{ \AA}$ and $a = 4.893 \text{ \AA}$, $c = 27.66 \text{ \AA}$ and $c = 26.64 \text{ \AA}$, respectively, and orthorhombic NbNi_3 phase with lattice constants of $a = 4.259 \text{ \AA}$, $b = 5.110 \text{ \AA}$ and $c = 4.559 \text{ \AA}$. Even though Nb-rich metastable phase has been reported to form during the primary crystallization step of the $\text{Ni}_{62}\text{Nb}_{38}$ amorphous phase, it was possible to confirm the formation of the metastable cubic phase: Ni and $\text{Nb}_{0.06}\text{Ni}_{0.94}$.

Investigations have revealed different type of fracture morphologies on the ribbon's cross section (Figs. 5, 6). Investigations of ribbons fractures showed their ductile character with vein pattern morphology, typical for amorphous alloys of high strength and ductility (Figs. 5, 6).

Observed veins show a diverse configuration and density (area A). From the air-side surface, smooth area with slight faults is observed (area B), whereas on the side surface of the sample in the immediate vicinity of the wheel-side surface (area C), the narrow parallel faults as a result of the occurrence of shear bands, are visible. Shear bands can be locally contorted and may have different thickness of the interlayer. The fracture morphologies show characteristics associated with the nature of fracture ductile amorphous metals. The fracture morphologies reveal characteristics associated with the nature of fracture ductile metal amorphous materials [34, 35].

The obtained results of EDX microanalysis of chemical composition examined by scanning electron microscope (SEM) show conformity with assumption of the chemical composition of the studied ribbon specimen (Fig. 5b–d). No oxygen has been observed. The EDX analysis demonstrated the presence of alloying elements: $\text{Ni} = 61.6 \pm 1.8$ and $\text{Nb} = 38.4 \pm 1.7 \%$ on the sample's air-side surface (A), the upper surface (B) and the lower surface (C) (Fig. 5b–d).

Conclusions

Based on the XRD pattern and DSC trace, it is concluded that the as-prepared $\text{Ni}_{62}\text{Nb}_{38}$ alloy ribbon is glassy alloy. The structure of the air-side surface and the wheel-side surface of ribbons cast on a smooth wheel surface is amorphous.

The parameters associated with GFA, i.e.: ΔT_x , T_{fg} , γ , R_c , Z_c are about 32 K, 0.582, 0.381, 207.29 K s^{-1} and 2.22 mm indicate the high GFA of $\text{Ni}_{62}\text{Nb}_{38}$. The parameter γ could be used as a useful guideline to identify the best glass former of Ni–Nb or even other binary alloys. The achieved parameters are significance for the future progress in research of this group of materials.

The crystallization behaviour of the $\text{Ni}_{62}\text{Nb}_{38}$ alloy has two-stage character. Crystallization peaks of the ribbons are observed in DTA trace with onset temperatures of $T_{x1} = 930$ and $T_{x2} = 982$ K, respectively. The crystallization products in the ribbons heated to 1023 K are the metastable cubic phase: Ni and $\text{Nb}_{0.06}\text{Ni}_{0.94}$ and a mixture of rhombohedral Nb_7Ni_6 and $\text{Nb}_{6.5}\text{Ni}_{6.5}$ phases and orthorhombic NbNi_3 phase.

The fractures of the cast $\text{Ni}_{62}\text{Nb}_{38}$ alloy ribbons after decohesion have different character dependent on regions of investigated. Ductile fracture with vein pattern morphology and smooth fracture with areas of shear bands has been observed.

Acknowledgements This work was financially supported with statutory funds of Faculty of Mechanical Engineering of Silesian University of Technology in 2015.

Open Access This article is distributed under the terms of the Creative Commons Attribution 4.0 International License (<http://creativecommons.org/licenses/by/4.0/>), which permits unrestricted use, distribution, and reproduction in any medium, provided you give appropriate credit to the original author(s) and the source, provide a link to the Creative Commons license, and indicate if changes were made.

References

- Hossain MS, Pandey AK, Tunio MA, Selvaraj J, Hoque KE, Rahim NA. Thermal and economic analysis of low-cost modified flat-plate solar water heater with parallel two-side serpentine flow. *J Therm Anal Calorim.* 2016;123:793–806.
- Souri D, Salehizadeh SA. Glass transition, fragility, and structural features of amorphous nickel–tellurate–vanadate samples. *J Therm Anal Calorim.* 2013;112:689–95.
- Dobrzański LA, Tański T, Dobrzańska-Danikiewicz A, Jonda E, Bonek M, Drygała A. Structures, properties and development trends of laser-surface-treated hot-work steels, light metal alloys and polycrystalline silicon, Laser surface engineering: processes and applications. Woodhead Publ Ser Electron Opt Mater. 2015;65:3–32.
- Klement W, Willens RH, Duwez P. Non-crystalline structure in solidified gold-silicon alloys. *Nature.* 1960;187:869–70.
- Suryanarayana C. Bulk metallic glasses. London: CRC Press Taylor & Francis Group Boca Raton; 2011.
- Inoue A, Hashimoto K. Amorphous and nanocrystalline materials: preparation, properties and applications. Berlin: Springer; 2001.
- Lesz S, Szewczyk R, Szewieczek D, Bienkowski A. The structure and magnetoelastic properties of the Fe-based amorphous alloy with Hf addition. *J Mater Process Tech.* 2004;157–158:743–8.
- Wang WH, Dong C, Shek CH. Bulk metallic glasses. *Mater Sci Eng.* 2004;R44:45–89.
- Inoue A. High strength bulk amorphous alloys with low critical cooling rates. *Mater Trans JIM.* 1995;36:866–75.
- Inoue A. Bulk amorphous and nanocrystalline alloys with high functional properties. *Mater Sci Eng.* 2001;A304–306:1–10.
- Inoue A, Shen BL, Chang CT. Fe- and Co-based bulk glossy alloys with ultrahigh strength of over 4000 MPa. *Intermetallics.* 2006;14:936–44.
- Wang D, Li Y, Sun BB, Sui ML, Lu K, Ma E. Bulk metallic glass formation in the binary Cu–Zr system. *Appl Phys Lett.* 2004;84(20):4029–31.
- Pu J, Wang JF, Xiao JZ, et al. Formation of Pd₈₂Si₁₈ bulk metallic glass and its crystallization. *J Huazhong Univ Sci Tech.* 2003;31:69–72.
- Yao KF, Ruan F, Yang YQ, et al. Superductile bulk metallic glass. *App Phys Lett.* 2006;88(12):122106.
- Li JH, Dai Y, Cui YY, Liu BX. Atomistic theory for predicting the binary metallic glass formation. *Mater Sci Eng.* 2011;R72:1–28.
- Xia L, Li WH, Fang SS, Wei BC, Dong YD. Binary Ni–Nb bulk metallic glasses. *J Appl Phys.* 2006;99:026103-1–3.
- Chen LY, Fu ZD, Zeng W, Zhang GQ, Zeng YW, Xu GL, Zhang SL, Jiang JZ. Ultrahigh strength binary Ni–Nb bulk glassy alloy composite with good ductility. *J Alloy Compd.* 2007;443:105–8.
- Lu ZP, Liu CT. A new glass-forming ability criterion for bulk metallic glasses. *Acta Mater.* 2002;50:3501–12.
- Novikov VN, Sokolov AP. Poisson's ratio and fragility of glass-forming liquids. *Nature.* 2004;431:961–3.
- Yang B, Liu CT, Nieh TG. Unified equation for the strength of bulk metallic glasses. *App Phys Lett.* 2006;88:221911-1–3.
- Zhang JL, Wang YM, Lu JX, Sheka CH, Wang Q, Dong C. Formation and mechanical properties of minor-Sb alloyed Ni₈Nb₅ bulk metallic glasses. *J Alloy Compd.* 2010;491:513–6.
- Lesz S, Griner S, Nowosielski R, Szewieczek D. The fracture morphology of amorphous Ni–Nb ribbons (in Polish). In: 17th Int Sci Conf Contemp Achiev Mechanics, Manuf Mat Sci. 2011; 65.
- Huang SC, Fiedler HC. Effects of wheel surface conditions on the casting of amorphous metal ribbons. *Metall Trans A.* 1981;12:1107–12.
- Nabiałek M, Pietrusiewicz P, Szota M, Dośpiał M, Jędryka J, Szota K, Lesz S. Evaluation of the microstructure and magnetic properties of Fe₇₃Me₅Y₃B₁₉ (where Me = Ti or Nb) amorphous alloys. *Arch Metall Mater.* 2012;57(1):223–7.
- Wang WH. Roles of minor additions in formation and properties of bulk metallic glasses. *Prog Mater Sci.* 2007;52:540–96.
- Sheng WB. Evaluation on the reliability of criterions for glass-forming ability of bulk metallic glasses. *J Mater Sci.* 2005;40(18):5061–6.
- Du XH, Huang JC, Liu CT, Lu ZP. New criterion of glass forming ability for bulk metallic glasses. *J Appl Phys.* 2007;101:086108-1–3.
- Hanawalt JD, Rinn HW. Identification of crystalline materials: classification and use of X-ray diffraction patterns. *Powder Diffraction.* 1986;1:2–6.
- Hanawalt JD. Manual search/match methods for powder diffraction in 1986. *Powder Diffraction.* 1986;1:7–13.
- Lee MH, Kim WT, Kim DH, Kim YB. The effect of Al addition on the thermal properties and crystallization behavior of Ni₆₀Nb₄₀ metallic glass. *Mater Sci Eng A.* 2004;375–377:336–40.
- Chang HJ, Park ES, Jung YS, Kim MK, Kim DH. The effect of Zr addition in glass forming ability of Ni–Nb alloy system. *J Alloy Compd.* 2007;434–435:156–9.
- Czeppe T. Mechanism and kinetics of nano-crystallization of the thermally stable NiNb(ZrTi)Al metallic glasses. *J Therm Anal Calorim.* 2010;101:615–22.
- Koseski RP. Manipulation of microstructure, phase evolution, and mechanical properties by devitrification of andesite for use as proppant, in materials science and engineering. University Park: The Pennsylvania State University; 2008. p. 239.
- Szewieczek D, Tyrlik-Held J, Lesz S. Changes of mechanical properties and fracture morphology of amorphous tapes involved by heat treatment. *J Mater Process Tech.* 2001;109:190–5.
- Korzniakova G, Czeppe T, Korznikov A. Structure and properties of Ni-based amorphous ribbons consolidated by high pressure torsion. *Rev Adv Mater Sci.* 2010;25:67–73.